Journal of Sound and Vibration (1997) **203**(5), 745–761

CONTROL OF AIRCRAFT INTERIOR NOISE USING GLOBALLY DETUNED VIBRATION ABSORBERS†

C. R. Fuller and J. P. Maillard

Vibration and Acoustics Laboratories, Virginia Polytechnic Institute and State University, Blacksburg, VA. 24061-0238 *U.S.A.*

AND

M. Mercadal and A. H. von Flotow

Hood Technology Corporation, Hood River, Oregon, 97031-9641 *U.S.A.*

(*Received* 8 *December* 1995, *and in final form* 2 *December* 1996)

A simplified analytical structural acoustics model of a propeller aircraft is developed to study the potential of mechanical vibration absorbers for reducing interior noise. The results show that globally detuning the absorbers to minimize an interior acoustic cost function gives attenuations of the order of 6–10 dB of the blade passage frequency interior noise when properly configured. The analysis also predicts that globally detuned absorbers consistently outperform tuned absorbers in which the base motion is directly minimized.

1. INTRODUCTION

The reduction of interior noise in aircraft still remains a challenge to aircraft designers and in recent years several advanced techniques have been considered. Tuned mechanical vibration absorbers designed to reduce the vibration of the aircraft fuselage, and hence its interior noise, have been developed and tested by a number of companies [1–3]. Sound reductions of the order of 8 to 10 dB in the fundamental blade passage frequency at cruise conditions with a weight penalty of about 25 kg have been reported. While this technique is fully passive and thus does not require any control energy, it suffers from a loss in performance when the absorbers are off-resonance, i.e., the propeller rotational speeds vary from the design point. A suggested solution to this problem would be to use absorbers whose properties could be adapted in order to track and remain tuned to the varying disturbance frequency.

Fully active solutions have also been considered. Recent flight tests have demonstrated the potential of an active control system termed Active Noise Control (ANC), which uses an array of acoustic control sources and error microphones distributed throughout the cabin space [4, 5]. Emerging commercial systems have been installed in aircraft such as the SAAB 340 or SAAB 2000 and typically comprise of 24–36 optimally located loudspeakers in conjunction with 48–72 error microphones. The total weight is around 70 kg for a 10 dB attenuation in the propeller fundamental frequency. Each speaker has a maximum power consumption of 25 Watts and approximately 1 km of wire is required in the SAAB 2000. The total power consumption of the system is approximately 300 Watts. The active noise control approach generally requires many control transducers. In addition, the performance tends to roll off at the higher harmonics of the propeller noise. An alternative,

†Paper originally presented at the 1st Joint CEAS/AIAA Aeroacoustics Conference, Munich, June, 1995.

0022–460X/97/250745 + 17 $25.00/0/sv960867

fully active approach is to use fuselage mounted vibration actuators in conjunction with interior microphones [6, 7]. This technique, termed Active Structural Acoustic Control (ASAC), is not as well developed or tested as ANC but shows potential to significantly reduce the number of required control transducers. Calculations estimate that a 12 actuator/24 sensor system would provide around 25 dB of attenuation with a weight of 18 kg (using inertial shakers) and consume approximately 150 Watts of electrical power. However, important disadvantages compared to ANC are a requirement for a larger control authority (or force/stroke output of the control actuator) and a possible increase in the fuselage vibration.

In this paper an analytical investigation of the potential of a system is outlined which is configured to combine some of the advantages of the above approaches. The system consists of multiple vibration absorbers whose properties can be electronically adjusted (an adaptive absorber) attached to an elastic cylindrical structure representative of an aircraft fuselage. The adaptive absorbers are configured to have resonances on or very near the disturbance frequency and thus can exert significant reactive force with a low system mass and a very low power consumption. Perfectly tuning the individual absorbers to the disturbance frequency would result in a large attenuation of the cylinder motion at the absorber attachment point. Previous studies on ASAC applied to aircraft fuselages have shown that minimizing the fuselage vibration often does not perform as well as directly minimizing the coupled interior acoustic field for low frequency disturbances. This observation suggests the concept of the system to be investigated in this paper; the properties of the absorbers are globally adapted in order to minimize a cost function based upon interior acoustic levels. In effect the absorbers are *globally detuned* so as to minimize selected cylinder structural modes in a distributed sense as opposed to minimizing the vibration under their mount points. These selected cylinder modes are well coupled to the interior acoustic field and thus reduction of the sound field throughout the interior space is ensured.

The analysis begins with a brief review of mechanical absorbers and approximate design formula. The analytical model of a representative aircraft fuselage with attached adaptive absorbers and the coupled interior acoustic field is outlined. The optimization technique for globally detuning the absorbers is summarized. Results are then presented for optimally tuned and globally detuned absorbers and compared for performance advantages. Finally, conclusions of the work are presented.

2. ANALYSIS

In this section the analytical model used to evaluate globally detuned absorbers for reduction of interior noise is outlined. Before the fuselage model is developed it is useful to review tuned mechanical absorbers.

2.1. TUNED MECHANICAL ABSORBERS—AN OVERVIEW

Consider a mass mounted on a moving base through a spring/dash-pot mechanism as shown in Figure 1. The connecting system is considered infinitely rigid in all but one direction, normal to the axis of the main surface whose motion is to be suppressed. The mechanical impedance of such a system, Z_a, is given by

$$Z_a = M\mathrm{j}\alpha\omega_r\left[\frac{1+\mathrm{j}\alpha/Q}{1-\alpha^2+\mathrm{j}\alpha/Q}\right], \tag{1}$$

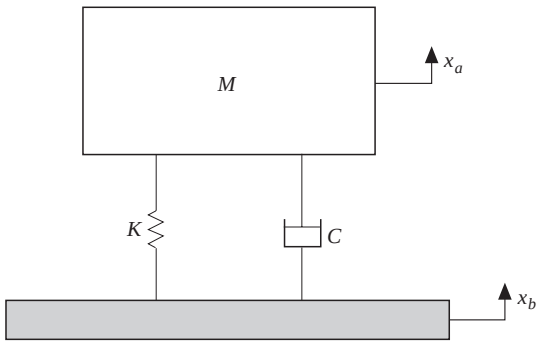

Figure 1. Mechanical vibration absorber schematic.

where M is the mass of the absorber, ω_r is the natural frequency of the absorber given by $\omega_r = \sqrt{K/M}$ and α is the ratio between the disturbance frequency and the natural frequency of the absorber, $\alpha = \omega/\omega_r$. The quality factor Q of the absorber is related to the damping and thus the sharpness of the absorber response peak at resonance and is defined as

$$Q = M\omega_r/C, \tag{2}$$

where C is the damping constant of the dash-pot. Note that with no damping ($C = 0$), the system's tuned impedance ($\alpha = 1$) becomes infinite and purely imaginary. In this case, the absorber will theoretically suppress the vibrations of anything it is attached to by exerting an infinitely large reactive force on the structure. Generally then, vibration absorbers with high MQ do not primarily "absorb" energy and the name is a misnomer. The expression of equation (1) can be approximated near resonance and for high-Q systems by

$$Z_a \approx M\mathrm{j}\alpha\omega_r/(1 - \alpha^2 + \mathrm{j}\alpha/Q). \tag{3}$$

It can be seen from equation (3) that the mechanical impedance of the absorber at resonance is $Z_a \approx M\omega_r Q$. Thus, operated at resonance, the dynamic impedance of the

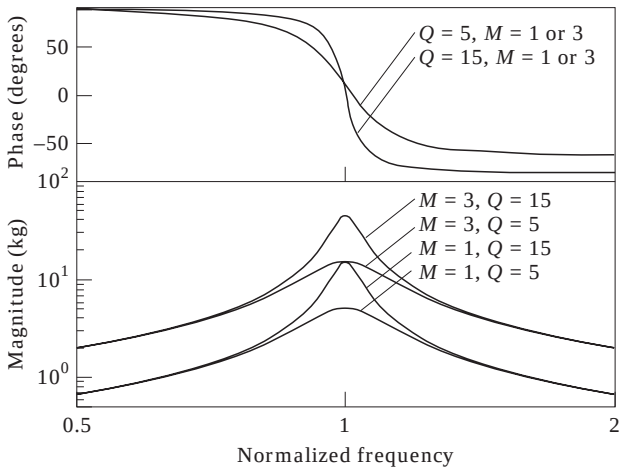

Figure 2. Normalized absorber impedance, Z_a/ω_r, as a function of M and Q.

absorber is Q times that resulting from a same mass rigidly mounted to the base. Figure 2 shows the magnitude and phase of the normalized absorber impedance, Z_a/ω_r, with unit of mass as a function of normalized frequency, ω/ω_r, for various values of M and Q. Note that the mechanical impedance of an absorber at resonance is a strictly increasing function of its MQ product (mass times quality factor). At resonance, the dynamic amplification factor of Q is a convenient low-mass method for gaining mechanical impedance (of the absorber). Off-resonance, unfortunately, there is no substitute for mass since the absorber impedance is strictly proportional to its mass. Given two absorbers which achieve the same dynamic impedance at resonance, the one utilizing a lower Q and a higher mass will therefore be more effective off-resonance (i.e., when it is detuned). Note, however, that even for low values of Q (e.g., $Q = 5$), the impedance of the absorber (and thus its effectiveness) drops rapidly off resonance. For example in the aircraft fuselage application with an absorber tuned for the propeller blade passage frequency (BPF), at twice this frequency (2 BPF), the impedance is reduced by nearly a factor of 10.

It is also useful to derive the expression for the attenuation of the vibration of the base due to the absorber. The base structure is characterized by a free velocity with no absorber attached, v_{free}, and a mechanical input impedance at the attachment point, Z_b, which is a complex frequency dependent quantity which relates velocity and force (for example due to some disturbance) by $Z =$ force/velocity. If one now attaches an absorber, the total force applied to the base is the sum of the force resulting from the disturbance (which causes v_{free}) and the force exerted by the absorber back onto the base. Using the relationship for impedance one can express this equality as

$$Z_b v_{\text{base}} = Z_b v_{\text{free}} - Z_a v_{\text{base}}. \tag{4}$$

Hence the ratio of the base motion with the absorber to that without it can be written as

$$v_{\text{base}}/v_{\text{free}} = Z_b/(Z_a + Z_b). \tag{5}$$

This ratio must be minimized at the disturbance frequency to obtain the largest possible tonal attenuation. The denominator is constituted by the sum of two complex numbers, the modulus of which increases: (1) when the modulus of Z_a increases, (2) when the phase of Z_a better matches that of Z_b (then the moduli simply add). Referring to Figure 2, one clearly sees that the absorber's impedance modulus is maximized at resonance. The phase of the impedance is then 0°. Bringing the absorber's phase closer to that of the base requires operating off-resonance and thus at a smaller dynamic impedance. Very little is gained by detuning the absorber to try to match the phase: an absorber with a Q of 15 delivers, at best, 10% better performance (1 dB) when the base has either a mass of a spring like impedance (phase of $\pm 90^\circ$) and when Z_a and Z_b have comparable moduli. The tuned attenuation is, in that case, 3 dB. Should the base behave like a dash-pot, the attenuation would be 6 dB, since the phase of the base impedance is 0°. From this analysis, one concludes that a single absorber should be tuned to the disturbance frequency and that it should have a dynamic impedance large compared to the base impedance to be effective in attenuating base vibrations. The dynamic impedance at resonance is the product of the moving mass (which should be kept low for aircraft applications) and the quality factor: absorbers for aircraft applications should therefore be made with the highest possible quality factors. However, this also implies a rapid drop in performance if the disturbance frequency changes, thus suggesting the use of an adaptive tuned absorber whose resonance can track the disturbance.

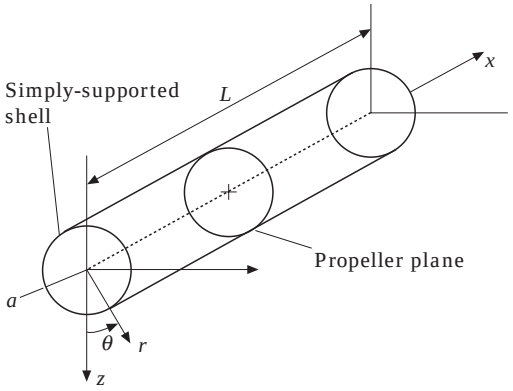

Figure 3. Co-ordinate system of the fuselage model.

2.2. FUSELAGE INTERIOR NOISE MODEL WITH VIBRATION ABSORBERS

In this analysis the aircraft fuselage dynamics and its acoustic behavior is modelled as a simply supported cylinder of length L, radius a, and thickness h as shown in Figure 3. The analysis is based upon a previous model developed by Silcox and Lester [8]. The cylinder is assumed to have rigid shear-diaphragm end caps. The input disturbance to the cylinder is represented by a harmonic, narrowband external pressure loading $p_d(x, \theta)\, e^{j\omega t}$ acting on the exterior of the cylinder. N vibration absorbers are mounted on the cylinder in order to alter the primary structural response due to the external pressure field. They can be modelled by a set of radially acting point forces, $F_i (i = 1, 2, \ldots, N)$. The amplitude F_i of the force exerted by the absorber on the structure is a function of the mechanical compliance of the ith absorber and the shell displacement at the mount location, (x_i, θ_i):

$$F_i = -Z_i^d \omega(x_i, \theta_i). \tag{6}$$

In the above equation Z_i^d relates the displacement of the ith absorber's base to the force acting back onto the base. It is defined as $Z_i^d = j\omega Z_a$, where Z_a is the mechanical impedance given in equation (1). The contribution of the N absorbers is expressed as a pressure input distribution of the form.

$$f^a(x, \theta) = \sum_{i=1}^{N} F_i \delta(x - x_i) \frac{\delta(\theta - \theta_i)}{a}, \tag{7}$$

where δ represents the Dirac delta function. The above distribution can be seen as the secondary "control" source while the external sound pressure field represents the primary "disturbance" source. Note that the secondary source is coupled to the cylinder displacement through the absorbers impedance $Z_i^d (i = 1, 2, \ldots, N)$.

Using standard thin shell theory [9] the normal displacement of the cylinder can be written as

$$\omega(x, \theta, t) = \left\{ \sum_{m=1}^{\infty} \sum_{n=0}^{\infty} W_{mn}^c \sin(\gamma_m x) \cos(n\theta) + \sum_{m=1}^{\infty} \sum_{m=1}^{\infty} W_{mn}^s \sin(\gamma_m x) \sin(n\theta) \right\} e^{j\omega t}, \tag{8}$$

where the complex coefficients, W_{mn}^c and W_{mn}^s, give the amplitude of the response of the cylinder in the (m, n)th vibration mode and $\gamma_m = m\pi/L$. Here m and n correspond to the modal order in the axial and circumferential direction, respectively.

In order to find the response of the system, it is convenient to expand $p_d(x, \theta)$ and $f^a(x, \theta)$ into series with the form of equation (8). Thus $p_d(x, \theta)$ can be written as (omitting $e^{j\omega t}$)

$$p_d(x, \theta) = \sum_{m=1}^{\infty} \sum_{n=0}^{\infty} P_{mn}^{d,c} \sin(\gamma_m x) \cos(n\theta) + \sum_{m=1}^{\infty} \sum_{n=1}^{\infty} P_{mn}^{d,s} \sin(\gamma_m x) \sin(n\theta). \tag{9}$$

A similar expression is applied to the force input distribution of the absorbers:

$$f^a(x, \theta) = \sum_{m=1}^{\infty} \sum_{n=0}^{\infty} F_{mn}^{c} \sin(\gamma_m x) \cos(n\theta) + \sum_{m=1}^{\infty} \sum_{n=1}^{\infty} F_{mn}^{s} \sin(\gamma_m x) \sin(n\theta). \tag{10}$$

In both of the above equations, the modal force amplitudes, $P_{mn}^{d,c}$, $P_{mn}^{d,s}$, F_{mn}^{c}, and F_{mn}^{s}, can easily be obtained by utilizing orthogonality of the shell mode shape functions [8]. For instance the absorber modal forces are found to be

$$F_{mn}^{c/s} = \frac{2}{L\epsilon_n \pi a} \sum_{i=1}^{N} F_i \sin(\gamma_m x_i) \{\cos/\sin\}(n\theta_i), \tag{11}$$

where $\epsilon_n = 2$ if $n = 0$ and $\epsilon_n = 1$ otherwise.

The complex amplitude coefficients for the coupled response are then expressed as

$$W_{mn}^{c/s} = H_{mn}^{c/s}(\omega) F_{mn}^{c/s} = H_{mn}^{c/s}(\omega)(P_{mn}^{c/s} + F_{mn}^{c/s}) \tag{12}$$

for both the sine and cosine circumferential distribution. The modal frequency response function is defined as

$$H_{mn}(\omega) = \gamma[(L_{11}L_{22} - L_{12}L_{21})/\det(\mathbf{L})]. \tag{13}$$

For the Donnell–Mushtari shell theory the L_{ij} coefficients of matrix $\mathbf{L}$ are defined as follows:

$$L_{11} = \Omega^2 - \xi_m^2 - [(1 - \nu)/2]n^2, \qquad L_{12} = L_{12} = [(1 + \nu)/2]n\xi_m, \qquad L_{13} = L_{31} = \nu\xi_m, \tag{14a–c}$$

$$L_{22} = \Omega^2 - n^2 - [(1 - \nu)/2]\xi_m^2, \qquad L_{23} = L_{32} = -n, \qquad L_{33} = \Omega^2 - 1 - \beta^2(\xi_m^2 + n^2)^2, \tag{14d–f}$$

where $\xi_m = \gamma_m a$. In equation (14), Ω is the non-dimensional disturbance frequency defined by $\Omega = \omega a/c_L$, the parameters γ and β are defined by $\gamma = -(1 - \nu^2)a^2/Eh$ and $\beta^2 = h^2/12a^2$. The longitudinal phase speed of the shell material is given by $c_L = \sqrt{E/\rho_s(1 - \nu^2)}$, where E, ρ_s and ν are the elastic modulus, density, and Poisson ratio of the shell material, respectively. Structural damping is included by adding a small imaginary part to the material's elastic modulus, $E_d = E(1 + j\eta_s)$, where η_s represents the structural damping factor which is valid for harmonic response.

In practice, fuselages are constructed from a skin, longerons and frames which are usually modelled using a smeared approach. However, this approach leads to a dynamic model which is overly soft and significantly alters the response of the system to forces due to disturbances such as actuators and absorbers. In this analysis an approach similar to that of Nelson *et al*. [10] is used to incorporate the bending and torsional stiffness due to

longerons and frames by adding correction terms to the Donnell–Mushtari equations. The L_{33} entry given in equation (14) is modified as follows:

$$L_{33} = \Omega^2 - 1 - \beta^2(\mu_a \xi_m^4 + \mu_h n^4 + 2\mu_t \xi_m^2 n^2), \tag{15}$$

where the correction factors, μ_t, μ_a, and μ_h are given in Table 1. Including the density correction factor, μ_m, the longitudinal phase speed also becomes

$$c_L = \sqrt{E_d/\rho\mu_m(1 - \nu^2)}. \tag{16}$$

A matrix notation is now introduced to solve for the coupled response of the system with absorbers. The infinite summations in the previous equations are approximated by finite summations including the first N_{circ} circumferential modes and N_{long} longitudinal modes. Taking into account both sine and cosine circumferential modes, the total number of modes is $N_{\text{mode}} = 2N_{\text{circ}}N_{\text{long}}$. Let $\mathbf{q}$ represent the column vector of modal displacement amplitudes, W_{mn}^c and W_{mn}^s, $\mathbf{f}$ the column vector of absorber modal forces, F_{mn}^c and F_{mn}^s, and $\mathbf{f^a}$ the column vector of forces in the absorbers, F_i. Equation (6) can be written as

$$\mathbf{f^a} = -\mathbf{Z\Phi^a q}, \tag{17}$$

where $\mathbf{Z}$ is a $N \times N$ diagonal matrix containing the compliance terms $Z_i^d (i = 1, 2, \ldots, N)$, and $\mathbf{\Phi^a}$ is a $N \times N_{\text{mode}}$ matrix relating the modal amplitudes W_{mn}^c and W_{mn}^s to the radial displacements at the absorber locations, $\mathrm{w}(x_i, \theta_i)$. Now the absorber forces, F_i, are expanded in terms of the cylinder mode shapes (equation (11)) to yield the absorber modal forces, F_{mn}^c and F_{mn}^s. This is written in matrix notation as

$$\mathbf{f} = \mathbf{\Psi^a f^a}, \tag{18}$$

where $\mathbf{\Psi^a}$ is a $N_{\text{mode}} \times N$ matrix. Let $\mathbf{H}$ be the diagonal matrix containing the modal transfer functions $H_{mn}(\omega)$. Using equation (17) and equation (18), equation (12) is rewritten as

$$\mathbf{q} = \mathbf{Hp} - \mathbf{H\Psi^a Z\Phi^a q}, \tag{19}$$

where $\mathbf{p}$ is the column vector of external pressure modal components, $P_{mn}^{d,c}$ and $P_{mn}^{d,s}$. The displacement modal amplitudes of the coupled shell-absorber system are solutions of the linear system.

$$\mathbf{q} = \mathbf{A}^{-1}\mathbf{Hp}, \tag{20}$$

where

$$\mathbf{A} = \mathbf{I} + \mathbf{H\Psi^a Z\Phi^a}. \tag{21}$$

It should be mentioned that the matrix $\mathbf{A}$ is not diagonal, i.e., the presence of the absorbers yields a coupling between the cylinder structural modes. With no absorbers, the cylinder

TABLE 1

Density and stiffness correction factors

Term	Expression
Density	$\mu_m = 1 + A_F/hS_F + A_L/hS_L$
Torsion	$\mu_t = hD_L^3/(h^3 S_L/3)$
Axial bending	$\mu_a = 1 + (1/L_S S_L)(I_L + (D_L^2/4)[hS_L A_L/(hS_L + A_L)])$
Hoop bending	$\mu_h = 1 + (1/I_S S_F)(I_F + (D_F^2/4)[hS_F A_F/(hS_F + A_F)])$

where: A_F, A_L = frame and longeron cross-section area, D_F, D_L = frame and longeron height, S_F, S_L = frame and longeron spacing, I_F, I_L = frame and longeron area moment of inertia about neutral axis, respectively and I_S = skin area moment of inertia per unit length about neutral axis

displacement modal amplitudes are simply obtained by setting the absorber compliance matrix to zero.

As described by Silcox and Lester [8], the interior acoustic pressure can be obtained by a mode matching technique. The interior acoustic response can be written (omitting $e^{j\omega t}$) as

$$p(x, r, \theta) = \left\{ \sum_{m=0}^{\infty} \sum_{n=0}^{\infty} P^c_{mn} J_n(k_r r) \cos(\gamma_m x) \cos(n\theta) \right.$$

$$\left. + \sum_{m=0}^{\infty} \sum_{n=1}^{\infty} P^s_{mn} J_n(k_r r) \cos(\gamma_m x) \sin(n\theta) \right\}, \tag{22}$$

where $k_r^2 = k^2 - \gamma_m^2$. The acoustic wavenumber k is given by $k = \omega/c$, where c is the speed of sound. Damping is introduced in the acoustic cavity by adding a small imaginary part to c, $c_d = c(1 + j\eta)$, where η is the acoustic damping factor. In order to find the amplitudes P^c_{mn} and P^s_{mn}, it is necessary to apply the media interface boundary conditions of continuity of normal particle displacement at the shell wall. As described by Silcox and Lester [8], this is most easily achieved by expanding the shell radial displacement in terms of the acoustic modes and then directly matching the new shell expansion coefficients and acoustic mode amplitudes. Using this procedure the interior pressure amplitudes are specified by

$$P^{c/s}_{mn} = [\rho\omega^2 / k_r J_n'(k_r a)] \hat{W}^{c/s}_{mn}, \tag{23}$$

which is valid for both the cos $(n\theta)$ and sin $(n\theta)$ circumferential distributions. In equation (23) the factor $\hat{W}^{c/s}_{mn}$ is specified by

$$\hat{W}^{c/s}_{mn} = \sum_{m'=1}^{\infty} \hat{C}_{m'm} W^{c/s}_{m'n}, \tag{24}$$

where the coefficients $\hat{C}_{m'm}$ are defined as follows:

$$\hat{C}_{m'm} = \begin{cases} \Delta^{(-)}_{m'm} + \Delta^{(+)}_{m'm}, & \text{if } m' \neq m; \\ 0, & \text{otherwise;} \end{cases} \qquad \Delta^{(\pm)}_{m'm} = \frac{1}{\pi \epsilon_m} \left[\frac{1 - \cos(m' \pm m)\pi}{m' \pm m} \right].$$

2.3. OPTIMIZATION OF THE STIFFNESS OF THE GLOBALLY DETUNED ADAPTIVE ABSORBERS

As discussed in section 2.1., the absorbers can be detuned by selecting a natural frequency different from the disturbance frequency. Let α_i be the detuning factor of the ith absorber defined in section 2.1. The absorber is tuned when $\alpha_i = 1$ and detuned otherwise. Practically, tuning or detuning is usually achieved by varying the stiffness of the absorber. In this section, the numerical procedure used to find the optimal detuning factors is presented. The optimization goal is to minimize some cost function related to the interior acoustic potential energy.

Two types of cost function were investigated. The first cost function is defined as the total kinetic energy associated with the normal vibrational field of the cylinder. It is defined in terms of the vector of modal amplitudes $\mathbf{q}$, as

$$J_{\text{struct}} = \tfrac{1}{2} \rho_s h a \omega^2 \mathbf{q}^{\text{H}} \mathbf{q}, \tag{25}$$

where $\mathbf{q}^{H}$ represents the Hermitian transpose of $\mathbf{q}$. The second cost function is an estimate of the total acoustic potential energy inside the shell. It is defined as

$$J_{\text{acous}} = \frac{1}{4\rho c^2}\int_V |p(x, r, \theta)|^2 \, \mathrm{d}V \approx \frac{1}{4\rho c^2}\frac{2\pi L}{N_x N_\theta N_r}\sum_{i_x=1}^{N_x}\sum_{i_\theta=1}^{N_\theta}\sum_{i_r=1}^{N_r} r_l |p(r_l, x_l, \theta_l)|^2. \tag{26}$$

As seen in equation (1), the absorber impedance is a non-linear function of the detuning factor α_i which requires implementing a non-linear parametric optimization procedure. The search for a minimum is constrained by setting upper and lower bounds on the detuning factors. The optimization algorithm used in the calculations is based on Sequential Quadratic Programming (SQP) techniques, also referred to as constrained quasi-Newton methods. An overview of SQP is found in references [11] and [12]. The constrained quasi-Newton method assumes the cost function has a unique minimum. In cases where several minima can be found within the constraints, the optimized solution is not guaranteed to yield the global minimum of the cost function. For the current system, plotting both structural and acoustic cost functions versus the tuning factors, α_i, reveals several local minima. In other words, the following results do not necessarily present the very best possible detuning configuration. To reduce the computational load involved in the optimization, an analytical expression was derived for the gradient of both cost functions with respect to the detuning factors, thus avoiding the need for finite difference approximations.

3. RESULTS AND DISCUSSION

3.1. CHOICE OF CYLINDER FUSELAGE MODEL PARAMETERS

For the following simulations we choose to model the fuselage structure of a BAe 748 propeller aircraft that was previously modelled by Thomas *et al*. [13, 14]. As discussed in section 2.2. of this paper, the fuselage is modelled as a simply supported, homogeneous cylinder of finite length with rigid end caps which is identical to that used by Thomas *et al*. However, for the present model the additional effects of the hoop and axial bending stiffness introduced by the stringers and frames as outlined previously are also included.

Thus, in addition to the mass of the stringers and frames being accounted for by "smearing" of their mass distribution, their stiffness is also included. Consequently, while most of the cylinder properties given in Table 2 are identical to those used by Thomas *et al*., the cylinder has a hoop and axial stiffness which is significantly different. A

TABLE 2

Parameters of the cylinder fuselage model

Parameter	Magnitude	Parameter	Magnitude
Cylinder length, L (m)	16	Frame:	
Cylinder radius, a (m)	1·3	Spacing S_F (m)	0·40
Cylinder thickness, h (m)	$1{\cdot}2 \times 10^{-3}$	Height, D_F (m)	0·09
Material density, ρ_s (kg/m^3)	2700	Area, A_F (m^2)	$1{\cdot}8 \times 10^{-4}$
Young's modulus, E (N/m^2)	$7{\cdot}1 \times 10^{10}$	Area moment of inertia, I_F (m^4)	$8{\cdot}7 \times 10^{-7}$
Poisson's ratio; v	0·31	Longeron:	
Speed of sound c (m/s)	343	Spacing, S_L (m)	0·40
Density of air, ρ (kg/m^2)	1·21	Height, D_L (m^2)	0·015
Structural damping, η_s	0·1	Area, A_L (m^2)	$0{\cdot}7 \times 10^{-4}$
Acoustic damping, η	0·1	Area moment of inertia, I_L (m^4)	$2{\cdot}7 \times 10^{-9}$

calculation of the input compliance of the cylinder gives values of the order of 0.2 μm/N at around 100 Hz, which is comparable to values reported in reference [1] for the SAAB 340 whose fuselage dynamic characteristics are similar to those of the BAe 748. When the value of stiffness assumed by Thomas *et al*. is used, the mobility obtained is of the order of 5 μm/N which is significantly higher. As discussed later, the decreased stiffness of the cylinder as in Thomas's model results in a higher modal density at the BPF and localized structural dimpling in response to a point force which has important implications on the use of tuned absorbers as compared to globally detuned absorbers. Also note that a damping factor of magnitude 0·1 was found to yield better correlation between the SAAB measurements and the present model compared to the 0·3 factor used by Thomas *et al*. Finally, the model includes 7 modes in the circumferential direction and 15 modes in the longitudinal direction ($N_{\text{circ}} = 7$, $N_{\text{long}} = 15$). Convergence tests showed the above modal truncation was sufficiently accurate at the frequencies of interest.

3.2. CHOICE OF THE PROPELLER PRESSURE DISTURBANCE FIELD

The disturbance pressure field discussed in section 2.2. is also based upon that generated by the right propeller of the BAe 748, as outlined by Thomas *et al*. [13]. In the axial direction the pressure amplitude decays exponentially in both directions from its peak in the propeller plane with a decay constant of 2 (i.e., the pressure is 1% of the maximum, 2·3 m away from the propeller plane). In the circumferential direction the pressure decreases linearly with angle from the maximum point and meets the fuselage at $\theta = 0^\circ$ and $\theta = 150^\circ$. The pressure peak is observed to occur at an axial distance of $x = 3{\cdot}5$ m (defining the propeller plane), $\theta = 85^\circ$ (which is the point of closest approach of the propeller) and has a maximum value of 150 Pa or 134·5 dB which is a representative pressure load for turboprop aircraft. Two discrete frequencies are considered; 88 Hz corresponding to the cruise blade passage frequency (BPF) of the BAe 748 and 176 Hz at twice the BPF. The calculated averaged sound pressure level in the fuselage with the previous cylinder parameters was 79·5 dBA at 88 Hz, which compares well with actual measured values in comparable "green" aircraft [1].

Although a realistic propeller acoustic footprint will have a varying phase in the circumferential direction due to the propeller trace velocity effects, the fuselage modal response in real aircraft is a standing wave pattern due to structural discontinuities such as the internal floor, etc. Therefore, to induce a standing wave pattern in the shell a uniform phase distribution was selected for the propeller footprint.

3.3. CHOICE OF THE ABSORBER AND THE COST FUNCTION FORM

For the following analysis, four absorbers were considered, positioned in the propeller plane as suggested by the results of references [1–3]. For most of the calculations the mass of each absorber was chosen to be 12·5 kg, giving a total absorber moving weight of 50 kg (relative to a cylinder weight of 645 kg), while the Q of the absorbers was chosen to be 15. The MQ of the system is thus 750 kg. The stiffness of the absorbers was set (in the case of tuned absorbers) or adapted (for detuned absorbers) by varying the value of the resonant frequency of each absorber. A preliminary analysis of the interior pressure field and the shell response without absorbers (see later) revealed that at 88 Hz the acoustic and shell vibration was dominated by circumferential modes of order $n = 1$ and 2 rotated by $-10{\cdot}66^\circ$ from the θ origin (see Figure 3). Thus the angular position of the four absorbers was chosen to be $-10{\cdot}66^\circ$, $+79{\cdot}33^\circ$, $+169{\cdot}33^\circ$, and $+259{\cdot}33^\circ$, corresponding to the anti-nodes of the rotated $n = 2$ mode. Note that the maximum in cylinder displacement does not correspond to the maximum in the pressure forcing function (which was at $\theta = 85^\circ$) due to the slight angular asymmetry in the propeller pressure forcing function.

Two different types of cost function were considered as the basis for the optimization scheme for the adaptive absorbers considered in section 2.3. The first cost function as defined in equation (25) represents tht total kinetic energy associated with the shell's normal vibration. The second cost function given in equation (26) is an estimate of the total acoustic potential energy radiated inside the shell. It is constructed by summing the squared modulus of the interior pressure evaluated over a grid of equally distributed points inside the shell and weighted by each point's radius. This cost function's estimate is based on 500 points distributed throughout the cylinder interior ($N_x = 10$, $N_\theta = 10$, $N_r = 5$). Note that 2040 points were used to compute the potential acoustic energy before and after optimization ($N_x = 20$, $N_\theta = 17$, $N_r = 6$). Reduction of the acoustic cost function thus implies a global reduction of the interior sound levels. The upper and lower limits imposed on the detuning factors, α_i (see section 2.3.), were set to 0·56 and 5, respectively. With these values, the absorber optimized natural frequencies are constrained to stay between $0{\cdot}2\omega$ and $1{\cdot}8\omega$, where ω is the disturbance frequency.

3.4. FREQUENCY OF $f = 88$ HZ (BPF)

For the first results the disturbance frequency was set to $f = 88$ Hz, corresponding to the propeller blade passage frequency of the BAe 748 system. Figure 4 and later figures show the amplitudes of the shell response for the three cases of uncontrolled, tuned, and detuned represented in bar diagram form from left to right, respectively, for each mode (m, n). The shell response consists of both a $\cos(n\theta)$ and $\sin(n\theta)$ component as shown in equation (8). The values plotted in Figure 4 are obtained from the square root of the sum of the squares of the amplitudes and thus represent the amplitude of a $\cos(n\theta)$ rotated to the position of maximum displacement. The results show that the shell response is dominated by $n = 1$ and 2 circumferential modal orders with a rotated origin at $\theta = -10{\cdot}66^\circ$. The corresponding interior pressure decomposition of Figure 5 shows that the pressure is dominated also by the $n = 1$ and $n = 2$ modes but at differing relative strengths due to the value of the cylinder structural acoustic coupling. The interior pressure

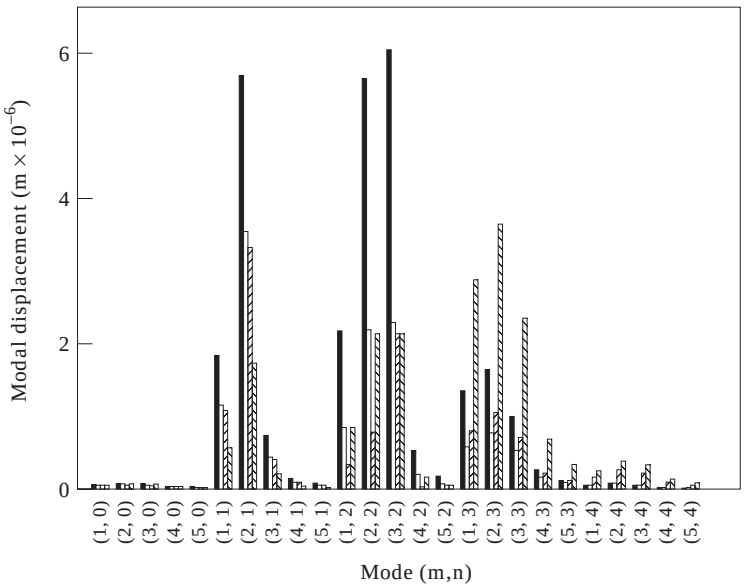

Figure 4. Structural response at 88 Hz: ■, uncontrolled; □, tuned; ▨, detuned, J_{struc}; ▧, detuned, J_{acous}.

amplitudes are decomposed at the shell wall (where it is maximum) and each (m, n)th component includes contributions from the higher order radial modal orders.

For the first test we use tuned absorbers with ω set to 88 Hz. Figures 4 and 5 show the corresponding shell and interior pressure field decompositions and all modes are seen to be reduced to some degree. To evaluate the performance of the tuned absorbers the kinetic energy of the shell system and the acoustic potential energy of the interior is calculated as outlined above. Note that a finer mesh of 2040 points was used to evaluate the change in acoustic potential energy. For the tuned absorbers the shell kinetic energy was reduced by 6·4 dB while the interior acoustic potential energy was reduced by 4·3 dB. The vibration reductions under each absorber were 19·3, 18·4, 17·5, and 32·1 dB corresponding, respectively, to the angular positions stated in section 3.3.

One now turns to the use of adaptive absorbers whose individual stiffness properties are globally adapted (in effect one detunes the absorbers) to reduce a chosen cost function. The first cost function chosen is the kinetic energy of the shell normal vibrations. The absorbers are detuned, to reduce the cost function, as described in section 2.3. The corresponding modal amplitudes are given in Figures 4 and 5. The results of the shell decomposition show that while the $n = 1$ and $n = 2$ modes have been reduced, in contrast to the tuned absorber, the $n = 3$ amplitudes have increased. However, Figure 5 shows that the corresponding modal pressure amplitudes have all been reduced. For this case the reduction in shell kinetic energy is 8·4 dB and acoustic potential energy is 5·0 dB. Thus, the use of globally detuned absorbers has led to an slightly increased interior sound reduction over the tuned absorbers. The mechanism of reduction is very similar to the phenomenon of "modal restructuring" first discussed in reference [15] for planar elastic radiators. The sound field due to the increased $n = 3$ modes combines destructively with $n = 1$ and $n = 2$ modes to lead to a further drop in sound levels. More explicitly, the increased $n = 3$ shell vibration levels lead to an overall shell response which is not as well coupled to the interior acoustic field as in the case of tuned absorbers. The ratio of the disturbance frequency to the detuned natural frequencies of the absorbers, $\alpha_i = \omega/\omega_r^i$, is

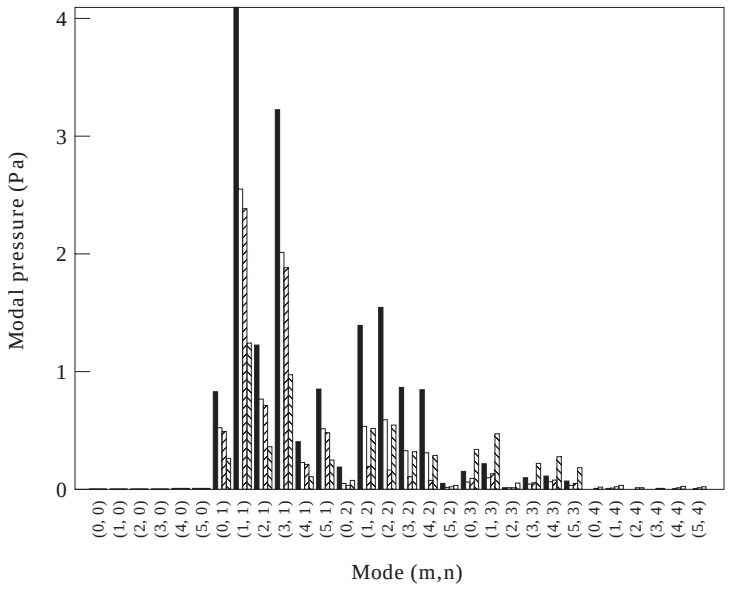

Figure 5. Interior acoustic response at 88 Hz: ■, uncontrolled; □, tuned; ▨, detuned, J_{struc}; ▧, detuned, J_{acous}.

0·95, 0·92, 0·95, and 5 for the respective absorber angular positions listed above. These values can be translated into a change of absorber stiffness using the relationship $K = M\omega^2$. Note that one of the above detuning factors has reached the upper limit set in the constrained optimization. Interestingly, a closer examination of this situation reveals that one of the optimally detuned absorbers is tending to zero stiffness (i.e., the absorbers are not present). Thus as well as optimizing the "active " component of the absorber, the approach of this paper also could be considered as simultaneously optimizing the "passive" component or mass distribution for example.

In the next case an interior acoustic potential energy is used as a cost function (a choice which seems the most logical since the objective is to globally reduce the interior sound levels). The shell and interior pressure modal amplitudes for this case are shown in Figures 4 and 5 along with the previous results. A similar trend is observed in the shell modal amplitudes as above. The $n = 1$ and $n = 2$ modes are reduced, however the $n = 3$ modal amplitudes are further increased over the results obtained with the cost function based on kinetic energy. The interior pressure modal amplitudes are all again reduced and to a further degree than when kinetic energy is used as a cost function. The reductions in the shell kinetic energy and the interior acoustic potential energy are 4·2 dB and 9·9 dB, respectively, when the acoustic potential energy is used as a cost function. The frequency detuning factors on the absorbers for this case are 0·74, 0·75, 1·06, and 0·62.

The results are summarized in Table 3. It is apparent that, at the BPF, globally detuning the absorbers leads to a significant improvement in reduction of the contained interior acoustic field over using individually tuned absorbers. This is an encouraging result especially for this "stiff" model where the shell modal density is lower at the BPF than previous fuselage studies of ASAC [13, 15]. Generally, better performance is achieved in ASAC when the modal density is higher.

3.5. FREQUENCY OF $f = 176$ HZ (2 BPF)

One now considers an identical set of simulation tests at twice the blade passing frequency or at the first harmonic of the propeller noise. Figures 6 and 7 show the modal amplitudes of the shell and interior pressure response at this higher frequency in the same format as previously. Also shown are the amplitudes with tuned absorbers and when globally detuned absorbers are used in conjunction with an interior acoustic potential energy cost function. The reductions in the acoustic potential energy for the test cases are summarized in Table 4. At this higher frequency the reduction in sound is not nearly as high as at $f = 88$ Hz. However, the globally detuned absorbers with both structural and acoustic based cost functions still perform better than tuned absorbers. Note that the two cost functions result in the same level of reductions. This suggests that vibration suppression rather than modal restructuring is the main mechanism of control at this frequency.

TABLE 3

Attenuation of shell kinetic energy and interior acoustic potential energy $f = 88$ Hz, $MQ = 750$ kg

	Δ Shell K.E. (dB)	Δ Acoustic P.E. (dB)
Tuned	6·4	4·3
Detuned (J_{struct})	8·4	5·0
Detuned (J_{acous})	4·2	9·9

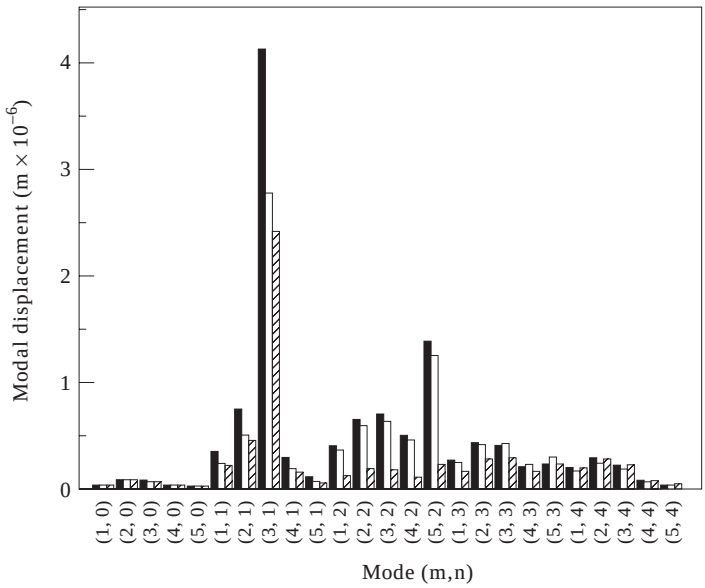

Figure 6. Structural response at 176 Hz using acoustic P.E. cost function: ■, uncontrolled; □, tuned; ▨, detuned, J_{acous}.

If one examines the results of Figures 6 and and 7 one sees that while the shell response is significant in the $n = 1, 2, 3$ and 4 modes, the interior acoustic field is dominated by the $n = 3$ circumferential mode positioned with a primary anti-node at $\theta = -21{\cdot}9^{\circ}$. Thus in order to reduce the coupled interior sound field, the dynamic absorbers should significantly reduce the $n = 3$ shell modal amplitude. Figure 6 reveals that the $n = 3$ shell modal amplitudes are only slightly reduced and thus the acoustic reduction is small. This behavior

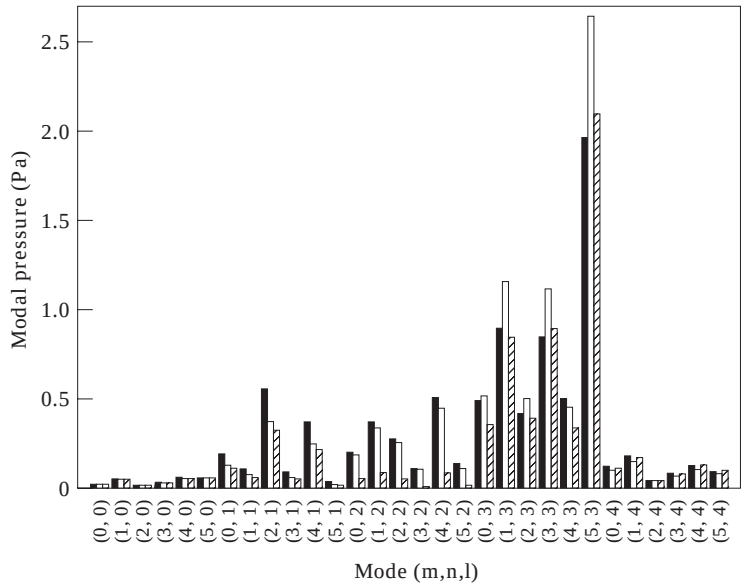

Figure 7. Interior acoustic response at 176 Hz using acoustic P.E. cost function: ■, uncontrolled; □, tuned; ▨, detuned, J_{acous}.

TABLE 4

Attenuation of shell kinetic energy and interior acoustic potential energy $f = 176$ Hz, $MQ = 750$ kg

	Δ Shell K.E. (dB)	Δ Acoustic P.E. (dB)
Tuned	1·3	−0·2
Detuned (J_{struct})	3·6	2·2
Detuned (J_{acous})	3·6	2·2

is most likely due to the fact that, in the present configuration, the absorbers are poorly positioned so as to couple into the $n = 3$ mode. Two of the absorbers are located within 10° of an anti-node of the rotated $n = 3$ modal distribution and are thus unlikely to globally modify its vibration to any significant degree. In general, the number of absorbers needs to be at least twice the modal order of the motion to be controlled (Nyquist theory) and this would imply the use of six, appropriately positioned absorbers. Thus to control the higher BPF components, a system would most likely be composed of many absorbers with lighter masses. In this case, on the basis of the discussion in section 2.1., it would be necessary to keep the absorber Q as high as possible. The detuning factors in these cases were 0·78, 0·94, 1·23, and 0·91 for the structural cost function and 0·88, 1·24, 0·96, and 0·74 for the acoustic cost function.

3.6. ABSORBERS WITH A REDUCED MQ = 480, $f = 88$ HZ (BPF)

For the next test the mass of each individual absorber is reduced from 12·5 kg to 8 kg giving a system MQ of 480 kg. The attenuations in the acoustic field are then evaluated using tuned absorbers and globally detuned absorbers in conjunction with an acoustic potential energy cost function. The results are summarized in Table 5 and demonstrate that even for this absorber system with lighter masses, the globally detuned system still provides reasonable attenuations of the interior field (8·3 dB) and outperforms the tuned absorbers by over 4 dB. However, as expected from the discussion of section 2·1., the lighter absorber system gives reduced attenuation than the heavier system considered previously. The detuning factors in these cases were 0·56, 0·88, 1·05, and 0·63 for the structural cost function and 0·83, 0·85, 1·11, and 0.79 for the acoustic cost function.

3.7. FREQUENCY OF $f = 88$ HZ $\pm$ 5% (ROBUSTNESS STUDY)

In this last test, a brief study of the robustness of both the tuned and globally detuned absorber system to a change in disturbance or operating condition was conducted. Here the absorbers are optimized using an interior acoustic potential energy cost function at the cruise BPF. The characteristics of the absorbers are fixed, the frequency of the disturbance is then varied by +5% (to 92·4 Hz) and −5% (to 83·6 Hz) and the reductions

TABLE 5

Attenuation of shell kinetic energy and interior acoustic potential energy $f = 88$ Hz, $MQ = 480$ kg

	Δ Shell K.E. (dB)	Δ Acoustic P.E. (dB)
Tuned	6·3	4·2
Detuned (J_{struct})	6·3	7·0
Detuned (J_{acous})	4·5	8·3

TABLE 6

Attenuation of shell kinetic energy and interior acoustic potential energy, $f = 88$ Hz $\pm$ 5%, $MQ = 750$ kg

	Δ Shell K.E. (dB)	Δ Acoustic P.E. (dB)
Tuned (+5%)	6·5 (6·4)	4·4 (4·3)
Detuned (J_{acous}) (+5%)	6·5 (4·2)	8·5 (9·9)
Tuned (−5%)	9·4 (6·4)	4·8 (4·3)
Detuned (J_{acous}) (−5%)	0·9 (4·2)	2·8 (9·9)

in the cost functions are evaluated. Results are shown in Table 6 where the reduction levels in parenthesis correspond to the 88 Hz disturbance frequency case (see Table 3). For the upper frequency (92·4 Hz), the reduction in the acoustic potential energy at $f = 92{\cdot}4$ Hz with the tuned absorbers is 4·4 dB (as compared to 4·3 dB at the cruise BPF) and 8·5 dB for the globally detuned absorbers (as compared to 9·9 dB for the cruise BPF). This last result is in contrast with the lower frequency (83·6 Hz) case where the reduction in acoustic potential energy for the globally detuned absorbers drops down to 2·8 dB. This reduction level is now lower than that obtained with the tuned absorbers (4.8 dB). The tuned absorbers appear less sensitive to small changes in the disturbance freuquency. However it should be noted that this robustness studies on tuned vibration absorber is in effect detuning them from the disturbance frequency. Future work will further investigate the shape of the cost function in order to study the system's robustness. However, in practice the absorbers would most likely be made adaptive in order to track the disturbance

4. CONCLUSIONS

An analytical model of the structural acoustic behavior of a propeller aircraft including vibration absorbers attached to the fuselage has been developed. The model was then used to study the potential of vibration absorbers for reducing interior noise. The results demonstrate that when the tuned absorbers are correctly configured, attenuation of 6–10 dB in the total interior acoustic potential energy possible. The model also demonstrated that globally detuning the absorbers to minimize an interior acoustic cost function gives improved attenuation over tuned absorbers. Further analysis indicated that the attenuations are relatively insensitive to small changes in the disturbance frequency at the blade passage frequency. The importance of the positioning of the absorbers was also shown.

ACKNOWLEDGMENT

The authors gratefully acknowledge the Office of Naval Research (Dr. Kam Ng, Technical Monitor).

REFERENCES

1. W. G. HALVORSEN and U. EMBORG 1989 *In Proceedings of the Business Aircraft Meeting and Exposition*, *Wichita*, *Kansas*, *April* 11–13, *SAE Paper* 89–1080. Interior noise control of the SAAB 340 aircraft.
2. E. H. WATERMAN, D. KAPTEIN and S. L. SARIN 1983 *In Proceedings of the Business Aircraft Meeting and Exposition*, *Wichita*, *Kansas*, *April* 12–15, *SAE Paper* 83–0736. Fokker's activities in cabin noise control for propeller aircraft.

3. H. J. Hackstein, I. U. Borchers, K. Renger and K. Vogt 1991 *In Proceedings of the DGLR/AIAA 14th Aeroacoustics Conference, Aachen, Germany, May* 11–14, *Paper No. DGLR/AIAA* 92-02-164. The Dornier 32 B Acoustic Test Cell (ATC) for interior noise tests and selected test results.
4. S. J. Elliott, P. A. Nelson, I. M. Stothers and C. C. Boucher 1989 *Journal of Sound and Vibration* **128**, 355–357. Preliminary results of in-flight experiments on the active control of propeller-induced cabin noise.
5. C. M. Dorling, G. P. Eatwell, S. M. Hutchins, C. F. Ross and S. G. C. Sutcliff 1989 *Journal of Sound and Vibration* **128**, 358–360. A demonstration of active noise reduction in an aircraft cabin.
6. C. R. Fuller and J. D. Jones 1987 *Journal of Sound and Vibration* **112**, 389–395. Experiments on reduction of propeller induced interior noise by active control of cylinder vibration.
7. M. A. Simpson, T. M. Luong, C. R. Fuller and J. D. Jones 1989 *AIAA Paper* 89–1074. Full-scale demonstration tests on cabin noise reduction using active vibration control.
8. R. Silcox and H. Lester 1989 *AIAA Paper* 89–1123. Propeller modelling effects on interior noise in cylindrical cavities with application to active control.
9. A. W. Leissa 1973 *Vibration of Shells*. NASA SP-288.
10. H. C. Nelson, B. Zapotowski and M. Bernstein 1958 *In National Specialists Meeting on Dynamics and Aeroelasticity*, Vibration analysis of orthogonally stiffened circular fuselage and comparison with experiment.
11. R. Flechter 1980 *Practical Methods of Optimization*. John Wiley; Volume 1 Constrained Optimization.
12. P. E. Gill, W. Murray and M. H. Wright 1981 *Practical Optimization*. London: Academic Press.
13. D. R. Thomas, P. A. Nelson and S. J. Elliott 1994 *Journal of Sound and Vibration* **167**, 91–111. Active control of the transmission of sound through a thin cylindrical shell, part I: the minimization of vibrational energy.
14. D. R. Thomas, P. A. Nelson and S. J. Elliott 1994 *Journal of Sound and Vibration* **167**, 113–128. Active control of the transmission of sound through a thin cylindrical shell, part II: the minimization of the acoustic potential energy.
15. C. R. Fuller, C. H. Hansen and S. D. Snyder 1991 *Journal of Sound and Vibration* **145**, 195–215. Active control of sound radiation from a vibrating rectangular panel by sound sources and vibration inputs: an experimental comparison.